catalysts

MDPI

Article

Synthesis and Characterization of Zinc Peroxide Nanoparticles for the Photodegradation of Nitrobenzene Assisted by UV-Light

Jesús Isaías De León Ramírez [1], Víctor Alfredo Reyes Villegas [1], Sergio Pérez Sicairos [2], Esteban Hernández Guevara [1], Mirna Del Carmen Brito Perea [1] and Bertha Landeros Sánchez [1,*]

[1] Faculty of Chemical Sciences and Engineering, Autonomous University of Baja California, Calzada Tecnológico 14418, Mesa de Otay, Tijuana 22390, Mexico; jesus.deleon@uabc.edu.mx (J.I.D.L.R.); victor.alfredo.reyes.villegas@uabc.edu.mx (V.A.R.V.); esteban.hernandez.guevara@uabc.edu.mx (E.H.G.); dbrito@uabc.edu.mx (M.D.C.B.P.)

[2] Center for Graduates and Research in Chemistry, National Technological Institute of Mexico Technological Institute of Tijuana, Apdo, Tijuana 22000, Mexico; sperez@tectijuana.mx

* Correspondence: bertha.landeros@uabc.edu.mx; Tel.: +52-664-265-4845

Received: 12 August 2020; Accepted: 5 September 2020; Published: 10 September 2020

Abstract: The contamination of both soil and water by nitrobenzene (NB) is a problem that has been studied, where several reactive agents have been developed for the degradation of this compound as well as different methods. Nanoparticles with semiconductive properties have been studied for organic compounds photodegradation due to their assistance in optimizing the degradation processes. Two of the most promising photocatalysts are ZnO and TiO_2 because of their optimal results. In the present work the performance of the zinc peroxide (ZnO_2) nanoparticles was evaluated. ZnO_2 nanoparticles were synthesized from zinc acetate and hydrogen peroxide using the Sol-Gel method under ultrasound assistance. The characterization was carried out by UV–Vis spectroscopy, infrared Fourier transform total reflectance (ATR-FT-IR) spectroscopy, Raman spectroscopy, X-ray diffraction (XRD), Zeta potential, dynamic light scattering (DLS), field emission scanning electron microscopy (FE-SEM), and Energy Dispersive X-ray spectroscopy (EDX). The experiments for the degradation of NB were carried out in a photoreactor with UV lamps of 254 nm at 25 °C, using a solution of nitrobenzene with the nanoparticles. The best conditions for NB photodegradation were 30 ppm (ZnO_2) and 15 ppm (NB) at pH 2, reaching up to 90% degradation in 2 h. The intermediates formed during the photodegradation of NB were identified by gas chromatography mass spectrometry.

Keywords: zinc peroxide nanoparticles; nitrobenzene; photodegradation; water purification

1. Introduction

Nitrobenzene (NB) is an aromatic molecule that causes toxicity in living organisms. Exposure can lead to absorption through different routes, such as dermal, inhalation or orally. When NB is absorbed into the systemic circulation, it causes methemoglobinemia, hepatoxicity, neurotoxicity, inhibition of liver enzymes, conjectured carcinogenicity and also has been found to cause genotoxicity in Drosophila [1–3]. This carcinogenic pollutant is widely used for the fabrication of different types of products, such as dyes, explosives, and pesticides [4]. NB has become a potential contaminant and of greater interest for its investigation due to the effects it can have on human beings [5–8]. The United States Environmental Protection Agency has listed NB as one of the most important pollutants. Nitrobenzene is a toxic agent that even at low concentrations can be a pollutant for the environment and living organisms [9]. Some agencies (National Institute of Environmental Health Sciences and Environmental Protection Agency) have focused their attention on NB, due to possible

carcinogenic effects and water contamination, which is limited to 17 ppm in lakes and streams to prevent ingestion of fish and water that could cause health problems [10].

In this regard, several treatment processes were reported for effective nitrobenzene removal, which can be achieved by physical and chemical methods such as electrochemical reduction, catalysis, ozonation, biodegradation, adsorption, and photocatalysis [11–17]. This last method is one of the most promising for the following reasons: (1) complete mineralization, (2) no waste disposal problem, (3) low cost and (4) only mild temperature and pressure conditions are necessary [18].

The successful use of H_2O_2 as a source of active oxygen for environmental decontamination and disinfection, as well as an oxygen source for biodegradation of organic pollutants, has been amply reported [19]. In the photocatalysis field, semiconductors are of great interest, especially when they are combined with H_2O_2 [20,21]. When a semiconductor through the effects of electromagnetic radiation generates an electron/hole pair, their redox potential needs to be sufficiently positive and negative for the hole and electron, respectively, to generate free radicals that could subsequently degrade an organic contaminant [18]. These free radicals could be generated from environmental O_2 instead of H_2O_2 if the needed redox potential is reached.

A technique involving a semiconductor photocatalyst and a contaminant has been used for the purification of air and water, which consists of the production of an electron/hole pair after illuminating the semiconductor with energetic enough photons [22]. It has also been seen that irradiation of a nano photocatalyst activity is enhanced through two synergistic mechanisms: the effect of plasmonic hot electrons and photothermal collective heating [23]. Titanium dioxide, TiO_2, is the most common semiconductor photocatalyst and has been used for the degradation of energetic compounds like NB when exposed to ultraviolet irradiation thanks to their large bandgap (e.g., 3.0–3.2 eV) [24–26]. In the field of photocatalysis, several materials have been investigated. One of the most promising candidates is ZnO due to its potential as a green environmental management system. The properties that stand out in this material are direct and wide bandgap in the spectral region near the UV rays, strong oxidation capacity, good photocatalytic property and large energy of free exciton binding. There is evidence that in some cases the coupling of a semiconductor can reduce the recombination of the electron–hole pair, increasing the charge carrier's lifetime by effects of charge separation. Lee et al. (2016) demonstrated a 25% improvement in the photodegradation efficiency of ZnO by coupling it with ZnO_2 [22].

ZnO_2 is also a semiconductor with a bandgap greater than that of ZnO. Nanocrystalline ZnO_2 material is an indirect semiconductor with an energy gap near 4.5 eV [27], although its real value has been reported to be between 3.3–4.6 eV [28]. ZnO/ZnO_2 composite has shown a superior photocatalytic activity as compared with either of its constituents (ZnO or ZnO_2). A trend was found to be correlated with the amount of ZnO_2 granules present on ZnO crystallites, at a higher concentration of ZnO_2 on the surface a higher specific surface activity was observed, suggesting that ZnO_2 alone could possess good photcalytic activity. However, an experiment using this ZnO_2 powder alone presented a low photocatalytic activity regardless of its synthesis process (hydrothermally treated or untreated). This was expected since the absorption wavelength of the material (300 nm) and the light used in the irradiation had the same maximum-intensity wavelength, reducing the efficiency of electron/hole pair generation. Also, a reduction of the excitons lifetime is expected since the material exhibited a poor crystallinity [29]. Despite the fact that peroxide materials are stable at low temperatures, and that the conduction band of ZnO_2 is higher than that of other catalysts, such as TiO_2, it has been proved that ZnO_2 continues to preserve its crystalline structure at high temperatures (below 120) [30], and its facile synthesis and non-toxic nature [31] give rise to considering it as a candidate. In addition, the conversion of ZnO_2 to ZnO that takes place through the photoreaction releases O^{2-} and ZnO [30], which is a material with a small bandgap [22]. These factors can favor degradation since the two materials (ZnO_2/ZnO) will be coexisting in the system [30], increasing the photon absorption range. This phase transition does not compromise its recycling and reusability since it has been shown that ZnO_2 is a material that is easy, quick and has a low cost to regenerate, conserving its efficient catalytic activity [28].

Due to the observations stated above, in this study we synthesized and tested a highly crystalline powder of ZnO_2 with a light source with a wavelength of 254 nm which could generate electrons and holes more efficiently than a light source of 300 nm. The sol-gel/sonochemical route was used to obtain ZnO_2 with certain characteristics (highly crystalline and in the nanoscale) to evaluate its performance as a photocatalyst. It has been observed that this method has been useful to synthesize particles with a consistent size and crystallinity, hence that is why this method was selected [31]. In addition, the material that we synthesized contains crystals of a size smaller than 10 nm, which can support to enhance the adsorption of NB molecules because of their high surface/volume ratio and in this way benefiting the degradation of NB. Another property of the manufactured nanoparticles is that having O_2 available can help create more reactive species that play a role in the photodegradation reaction. Hence, we selected the ZnO_2 catalyst as a model for studying the degradation profiles and its mechanism in nitrobenzene photodegradation.

2. Results and Discussion

2.1. Synthesis of ZnO_2 Nanoparticles

The Following reaction (Equation (1)) takes place in the preparation of nanoparticles of zinc peroxide [31]:

$$Zn(O_2CCH_3)_2 + H_2O_2 \rightarrow ZnO_2 + 2HO_2CCH_3 \quad (1)$$

The formation of ZnO_2 nanoparticles was confirmed through visual assessment due to the white color and further confirmed throughout the characterization.

2.2. Characterization of ZnO_2 Nanoparticles

2.2.1. UV-Vis Spectroscopy

Figure 1A shows the UV-Vis spectra of ZnO_2 with a maximum excitation band at 285 nm is in agreement with the data found in the literature, perceiving a slight shift which can be due to the size of the nanoparticle [32]. The comparison of this maximum with that of Drmosh et al. (2010), where a nanoparticle with a size of 3.7 nm exhibits an absorption band at 280 nm, supports the statement that the shifts of the maximum absorption are due to the quantum confinement effects that appear in the nanoscale. When the particle size decreases enough to present properties due to quantum confinement the bandgap of the particle increases, and its absorption shifts to a lower wavelength [33]. Additionally, in Figure 1A it is seen that the spectrum of the reactant (dotted line) has no characteristic absorption, unlike the product, where it is observed that the spectrum changes after the reaction, with a noticeable change in the UV-Vis spectrum. These properties indicate that a ZnO_2 phase is probably present.

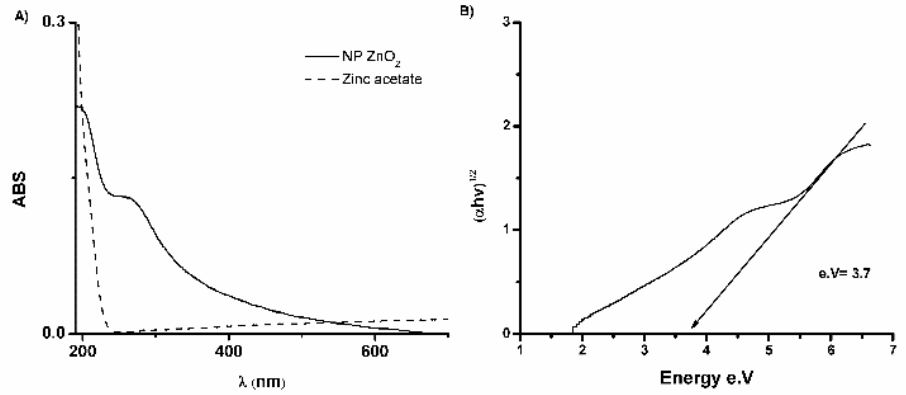

Figure 1. (**A**) UV-Vis spectrum of obtained ZnO_2 nanoparticles (black line) dispersed in water and comparison with reactant zinc acetate (dotted line) used for synthesis. (**B**) Indirect bandgap calculation for ZnO_2 nanoparticles.

As we know, the UV-Vis spectrum gives us information not only about the optical properties but also about the bandgap (Figure 1B). It is known that there is a strong hybridization between the states Zn-d and O-p. ZnO_2 is an indirect semiconductor with the upper part of the valence band located in Γ and the lower part of the conductance band located between Γ and R. For ZnO_2 the bandgap is 2.3 eV, however, it is generally underestimated by approximately 50–100% using density functional theory. Hence, the real value of the energy gap for ZnO_2 could be in the range of 3.3–4.6 eV, in agreement with the value calculated from spectrum [27]. The energy calculation of the bandgap (Equation (2)) can be calculated from the UV-vis absorption spectrum. The band interval energy was calculated using the Tauc method as seen below:

$$\alpha h\vartheta = C(h\vartheta - E_g)^n \quad (2)$$

where α is the absorption coefficient, hϑ is the incident energy, $n = 2$, C is a constant and E_g the optical bandgap. The graph was plotted with the values of $(\alpha h\vartheta)^{1/2}$ vs hϑ (E_g) for the calculation of the indirect band energy the linear part is extrapolated to zero with the abscissa (hϑ eV) [34,35]. The bandgap calculated was 3.7 eV (Figure 1B), which is within the range consulted in the literature [27].

2.2.2. Infrared Fourier Transform (FT-IR)

The FT-IR spectra of the ZnO_2 nanoparticles are shown in Figure 2A, with characteristic peaks at 667 cm^{-1}, 1022 cm^{-1}, 1405 cm^{-1} and 1565 cm^{-1}. The peak positions centered at 667 cm^{-1}, 1022 cm^{-1} and 1405 cm^{-1} may be due to the O–O bands corresponding to the peroxide (O_2^{-2}) ions of ZnO_2 nanoparticles. Another sharp absorption band of the ZnO_2 is observed located at 667 cm^{-1}, which corresponds to Zn–O vibration. As Verma et al. (2014) observed for ZnO_2 nanoparticles (average crystallite size of 151 nm) characteristic vibrations cause peaks at a wavenumber of 436 cm^{-1} for Zn–O bond, and 1040, 1334, and 1450 cm^{-1} for O–O bond [28]. The shifts of the wavenumbers could be due to the particle size, since there is evidence that suggest that the characteristic Zn–O vibration has a redshift as the particle size increases [32,36]. The difference of the crystallite size from those synthesized by Verma et al. (2014) and ours are 145 nm, with ours having an average of approximately 6 nm, supporting this evidence. In addition, the broad peak in the wavelength of 3384 cm^{-1} and the band 1565 cm^{-1} corresponds to characteristic stretches of the water molecule [37]. On the other hand, the bands shown in 1536 cm^{-1} and 1405 cm^{-1} may correspond to the vibrations of the reactant (zinc acetate) since they are characteristic of vibrations of C–O and C–C bonds [38]. This could be part of the reactant that did not react. It may sound logical that these are still present in the sample since the sample did not undergo any heat treatment, or could be arising from the absorption of atmospheric CO_2 on the surface of the nanoparticles [32]. In contrast, the % proportions of the atoms from the EDX analysis (Figure 3B) correlate with ZnO_2, with no extra oxygen coming from the acetate.

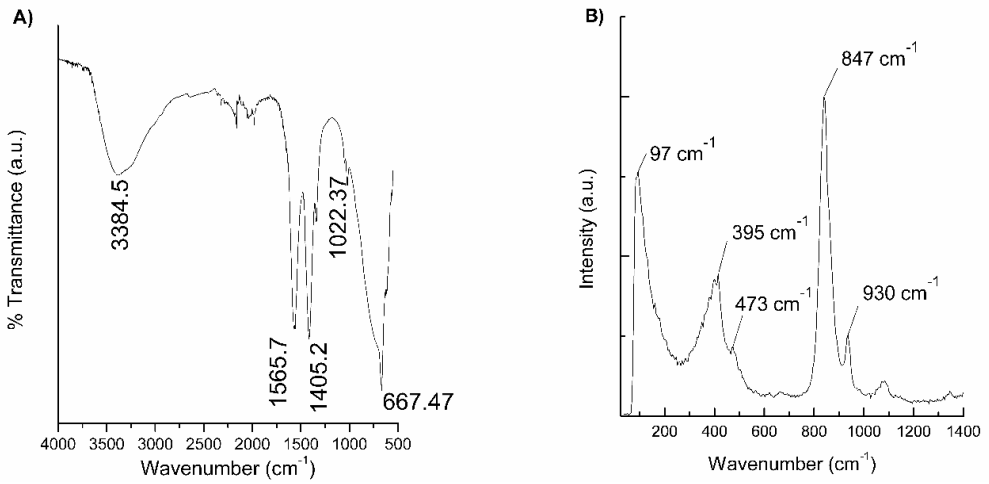

Figure 2. (**A**) Infrared Fourier transform (FT-IR) and (**B**) Raman spectrum for ZnO_2 nanoparticles.

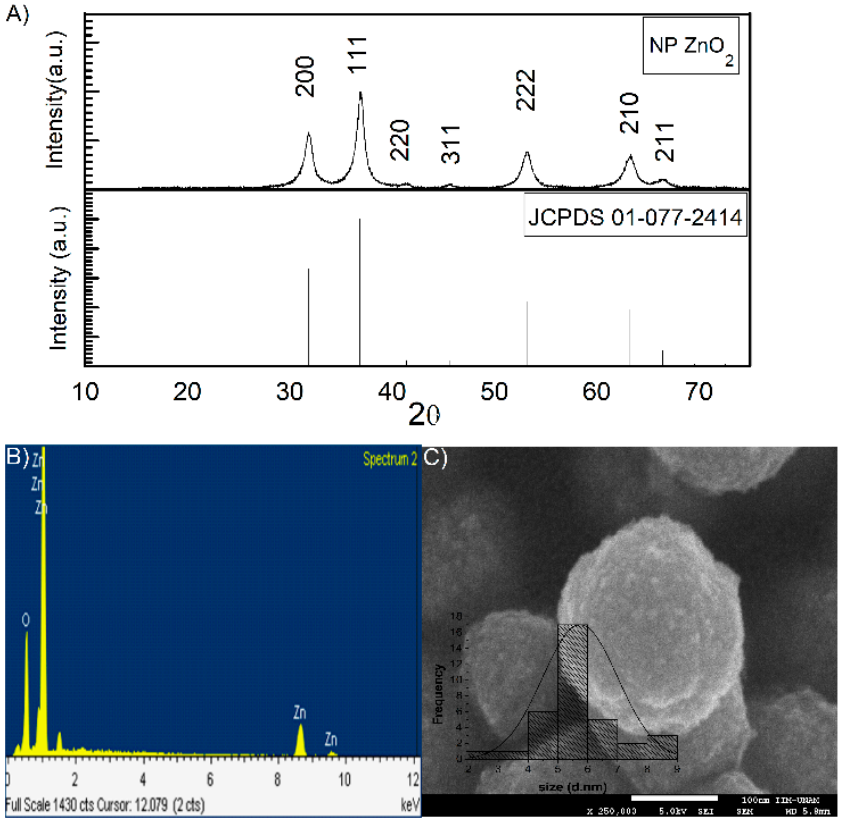

Figure 3. (**A**) X-ray diffraction (XRD), (**B**) Energy Dispersive X-ray spectroscopy (EDX) and (**C**) Scanning Electronic Microscope (SEM) image of ZnO_2 nanoparticles. The insert in the SEM image corresponds to a size distribution histogram of the ~8 nm crystals constituting a ~100 nm in diameter particle.

2.2.3. Raman Spectroscopy

The Raman spectra of ZnO_2 nanoparticles are shown in Figure 2B where 5 signals are present, at the positions of 97, 395, 473, 847 and 930 cm^{-1} respectively. These peaks are assigned to ZnO_2 according to the single phase observed in the XRD results. For instance, some peaks display low intensity and have been found in other peroxides [30] and the peaks at 847 and 930 cm^{-1} are in agreement with the Raman spectra of nanocrystalline ZnO_2 [39]. As for the most intense peak, a stretch mode of a O–O vibration that is not well resolved in the infrared spectrum is centered at approx. 840 cm^{-1} [30], suggesting that this mode could be ascribed to the band at 847 cm^{-1}.

2.2.4. X-ray Diffraction

To study the crystalline structure of the ZnO_2 nanoparticles, the powder was subjected to an X-ray diffraction analysis, obtaining the diffractogram shown in Figure 3A.

Where it is observed that all the peaks fit perfectly to the data found in the JCPDS reference (01-077-2414) that belongs to a cubic structure of ZnO_2. For the calculations of lattice parameter, cell volume and atomic radius the following formula (Equation (3)) was used:

$$d_{hkl} = \frac{a}{\sqrt{h^2k^2l^2}} = \frac{n\,\lambda}{2\,\sin\,\theta} \quad (3)$$

where hkl are the miller indices of the plane, *n* the diffraction order (commonly given as 1), λ is the wavelength (1541 A. CuKα) and θ is the Bragg diffraction angle of the plane [40]. These calculations are shown in Table 1 where we calculated, the typical characteristics of the cubic structures. For the crystal size, the Scherrer equation was used [41,42] obtaining a crystal size of approximately 6 nm.

Table 1. X-ray diffraction calculated ZnO_2 crystal structure parameters.

2θ	HKL JCPDS			Lattice Parameter (Å)	Atomic Radius (Å)	Cell Volume (Å^3)
37	2	0	0	4.86	2.43	115
31	1	1	1	4.91	2.45	118
53	2	2	0	4.87	2.43	115
63	3	1	1	4.87	2.43	115
66	2	2	2	4.87	2.43	115
41	2	1	0	4.89	2.44	117
45	2	1	1	4.88	2.44	116

2.2.5. Scanning Electronic Microscope (SEM) and Dynamic Light Scattering (DLS)

In Figure 3B the typical EDX spectrum of ZnO_2 is shown. This indicates the composition of the sample which is formed by Zn and O (the atomic ratio Zn/O is 1:1.54), approaching that of the consulted bibliography [43], supporting the approximated chemical composition that could be estimated for ZnO_2 according to the obtained XRD results. As mentioned above the size of the crystals calculated by the Scherrer equation was about 6 nm, in Figure 3C we can observe a micrograph of a ZnO_2 nanoparticle where it can be seen that the particle (~100 nm) is made of small crystals which were measured to be of about 6 nm.

Figure 4A shows a photo taken with an accelerating voltage of 5 KeV and subjected to image analysis with the help of J-image software for the measurement of the particle diameter distribution, obtaining an average diameter of approximately 100 nm with a normal distribution. This confirms the DLS analysis (Figure 4B) from which we obtained a D_h of ~100 nm, meaning that we synthesized nanoparticle clusters of about 100 nm with a normal distribution made from small crystals of ~6 nm.

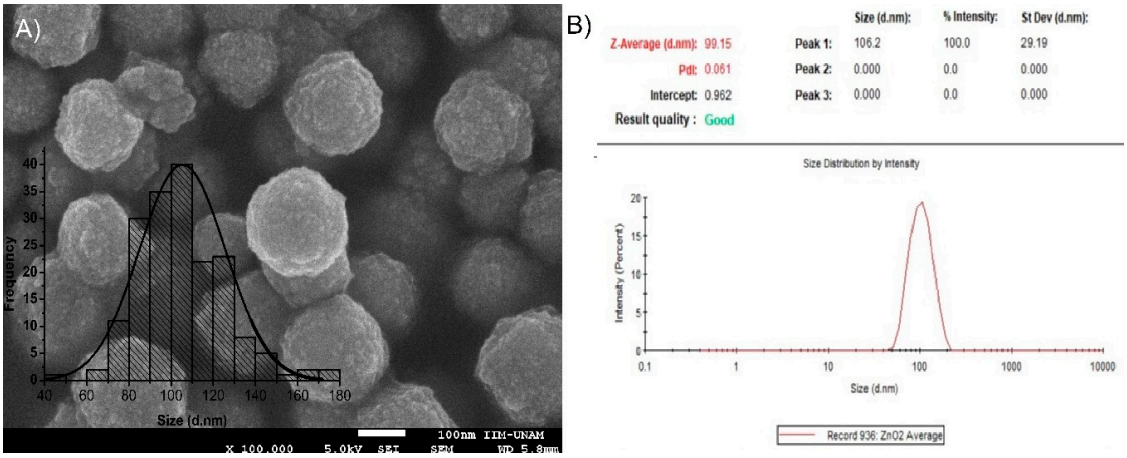

Figure 4. (**A**) SEM image with a gold coating and (**B**) hydrodynamic diameter (Dh) distribution by dynamic light scattering (DLS) analysis for ZnO_2 nanoparticles. The insert in the SEM image corresponds to a size distribution histogram of the ~100 nm in diameter particles.

2.2.6. Zeta Potential

Figure 5 presents the mean zeta potential profile at varying pH of ZnO_2 suspensions. This was calculated between a pH of 3 and 9 and the initial pH of the solutions was at pH 6.3, having an average zeta potential of +15 mV. As the pH increased, the zeta potential was found to decline gradually to a point of zero charges (PZC), which was measured between pH 7.5–8.0. After this point the solution showed an agglomeration. When reaching an alkaline pH of 9 the nanoparticles presented a charge of −18 mV ± 2. At alkaline pH, the dominant species are $Zn(OH)_2$ (aq), which could precipitate giving a new solid phase, $Zn(OH)_2$ (s). However, if the pH keeps rising, the global charge is mediated by the prevalence of negative species such as $Zn(OH)^-_3$ (aq) and $Zn(OH)^{2-}_4$ (aq), exhibiting a negative

surface [44]. By decreasing the pH of the solution below pH 7 it showed a dispersion region by increasing the zeta potential, thus having a dissolution region and agglomeration region agreeing with the consulted reference [45]. An isoelectric point (IEP) was observed at pH 3.2 (Figure 4), however two points at zero were detected, IEP at an acid pH and a PZC at an alkaline pH matching the reference [46].

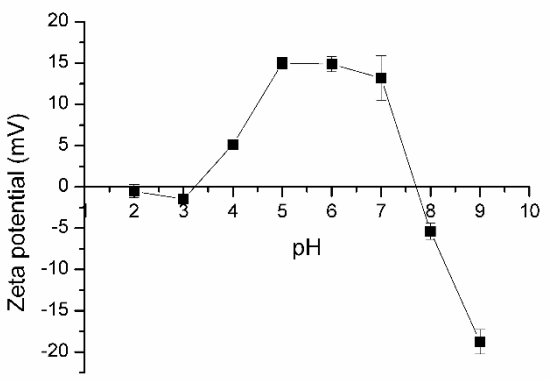

Figure 5. Effect of pH on the zeta potential measurement for ZnO_2 nanoparticles.

2.3. *Photocatalytic Degradation of Nitrobenzene*

2.3.1. Effect of Photocatalyst Concentration

Figure 6 presents the UV−vis absorption spectra of NB solution samples after photoreaction for different times. The typical spectrum of NB shows an absorption peak between 250 nm and 268 nm [47]. NB shows an absorption peak at 265, which decreased greatly in intensity as the UV exposure time increased in the presence of the ZnO_2 semiconductor. When an electron/hole pair is generated at a surface, several events can occur. They can recombine, irradiating the input energy as heat, cause collective plasmonic heating, produce hot electrons [23], enter in a metastable state or react with electron donors and acceptors adsorbed or near the surface of the particle [48–50]. These two last reasons are the main cause of the decrease in NB concentration. The following formula (Equation (4)) was used to obtain the percentage of degradation:

$$\text{Degradation } (\%) = [(\text{Co} - \text{Ct}/\text{Co})]\text{x}100 \quad (4)$$

where Co is the initial concentration or the initial absorbance of NB and Ct is the concentration or the absorbance of NB at a certain time 't' in minutes [51].

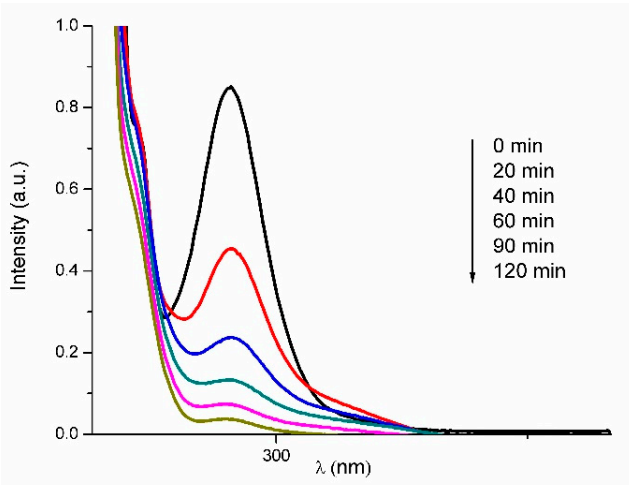

Figure 6. UV spectrum of aqueous nitrobenzene at different intervals for the photodegradation with ZnO_2 nanoparticles at optimum conditions.

NB absorbs at a wavelength close to the intensity of the lamps, which could suggest that the NB would degrade in the absence of the catalyst. However, the control experiment (Data not shown) with no photocatalyst was run and this event was discarded due to the low NB removal from solution, which was less than 10%.

Figure 7A shows the percentage of NB photodegradation at different ZnO_2 nanoparticle concentrations, being 20, 30 and 40 ppm with a NB% degradation of 53%, 63% and 57% respectively. It can be seen that increasing the concentration from 20 ppm to 30 ppm the NB degradation increased, confirming the positive influence of the increased number of ZnO_2 active sites on the process [52]. Therefore, the efficiency could be enhanced with the increase of ZnO_2 concentration because the total surface area available for nitrobenzene adsorption increased [53].

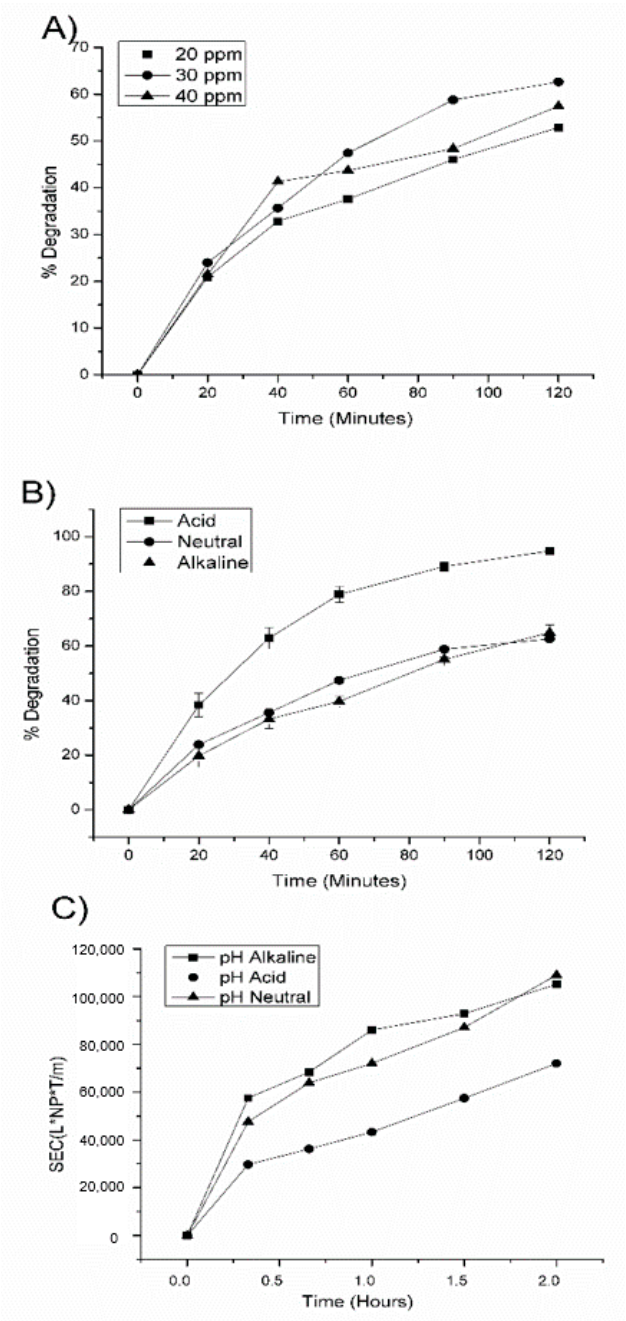

Figure 7. Percentage of nitrobenzene (NB) photodegradation by ZnO_2 nanoparticles at different (**A**) photocatalyst concentrations, (**B**) different initial pH value with 30 ppm of photocatalyst and (**C**) specific energy consumption for each reaction at different pH values.

On the contrary, increasing the concentration to 40 ppm had a repercussion on the degradation, the photocatalytic reaction decreases due to the decrease of light penetration and the increase of UV light scattering [54]. This decrease could also be attributed to a blocking effect taking place on the surface of the photocatalyst decreasing the efficiency of decomposition, as consequence of excessive O_2 ions acting as scavengers for OH radicals [55].

2.3.2. Effect of pH

The effect of pH on the photocatalytic activity (Figure 7B) was clear. The nanoparticles of ZnO_2 degraded 63%, 65%, and 98% for pH 7, 10 and 2 respectively, with pH 2 being the most effective. The reason may be that when the pH is 2.0, there is a strong Coulomb force between the surface of ZnO_2 nanoparticle and nitrobenzene, which is favorable for the adsorption of nitrobenzene on the surface of the photocatalyst [53]. The ZnO_2 colloid nanoparticles between a pH of 2 and 3 would, therefore, have a negative surface charge (Figure 5) and would be expected to experience a significant attraction to surfaces with a positive surface charge. The pKa of the NB is 3.98, where the anionic form dominates upon increasing the pH of the solution [56].

Therefore, at a pH between 2 and 3 ZnO_2 has a negative zeta potential and NB a positive charge under these conditions, which would boost attractions between nanoparticles and NB. Additionally, below pH 2 ZnO_2 nanoparticles release O_2 ions [57,58]. In the holes bridging O^- atoms with unit formal charge O^- are powerful oxidizing agents, which are capable of pulling electrons from adsorbed H_2O to yield H_2O^+, which can dissociate to yield a proton and the hydroxyl surface radical [49], as expressed in the following Equations (5)–(10):

$$ZnO_2 + hv \rightarrow e^-_{cb} + h^+_{vb} \quad (5)$$

$$e^-_{cb} + O_2 \rightarrow O_2^{\cdot -} \quad (6)$$

$$h^+_{vb} + OH^- \rightarrow OH^{\bullet} \quad (7)$$

$$h^+_{vb} + H_2O \rightarrow H_2O^+ \quad (8)$$

$$H_2O^+ \rightarrow OH^{\bullet} + H^+ \quad (9)$$

$$OH^{\bullet} + NB \rightarrow \text{Hydroxyl intermediates} + CO_2 + H_2O \quad (10)$$

Also photogenerated are electrons in the conduction band (e^-_{cb}) and holes within the valence band (h^+_{vb}), which can either recombine or reside in a trapped state or within the respective band. O_2 is an effective electron scavenger, forming either $O_2{}^-$ or $O_2{}^{-2}$ [48]. Newly formed superoxide radical anion (O_2^-) further reacts with water to generate hydrogen peroxide anions and increase the number of hydroxyl radicals, increasing the performance of the reaction [59]. In this manner, it improves the availability of contact and the amount of surface $OH^{\bullet}$ generated (Equations (5) and (7)) and increasing % degradation. These equations could be supported if the hydroxyl intermediates are identified.

Frequently, in both the literature and international standards, SEC is used as an energy performance indicator to evaluate or measure the performance of energy efficiency [60]. Figure 7C shows the energy efficiency of the effect of pH on the photocatalytic activity. At the optimal parameters (pH 2 and 30 ppm ZnO_2) and after 120 min of treatment, 97.7% of NB was degraded with a corresponding SEC of approx. 60,000 kWh/kg.

The photocatalytic activity of the prepared nanoparticles, compared with the most relevant reported photocatalysts for the degradation of NB (Table 2), had a high 98% removal. As shown in Table 2 our percentage of degradation (98%) is achieved in half or, in some cases, even at one quarter of the time (2 h) compared to the obtained degradation by other catalyst such as: TiO_2 nanotubes (50 mg) [61], $SrFeO_{3-\delta}$ (1000 ppm) [62], TiO (0.3% *w*/*v*) [63] and TiO_2 (50 mg) [10], which degraded the NB in solution with an efficiency of 100%, 99%, 98.5% and 98% in 4, 6, 4, 8 h respectively. Moreover, G–ZnO–Au NCs, see Table 2 [64], and (0.50%) Zn doped TiO_2 had a 98 and 97 percentage of degradation

in 2.3 and 2 h respectively, having very similar results as our synthesized nanoparticles. In short, we have synthesized ZnO_2 nanoparticles by a facile method capable of acting as a photocatalyst for the mineralization of NB as good as the catalyst reported in the literature or better. These novel findings contribute another option for the removal of this contaminant. The sol-gel/sonochemical method has proven to be useful for the synthesis of ZnO_2 nanoparticles as a photocatalyst, however it is necessary to study in more detail the synthesis factors that could indirectly influence the photocatalysis reaction efficiency, such as reactant ratios, sonication time, temperature, and drying methods, which could have an effect on the size and crystallization of the particles.

Table 2. Comparison of photocatalytic activity of ZnO_2 with the reported various catalysts for NB degradation.

Material	[Material]	[NB]	Time (h)	Type of Irradiation	NB Degradation (%)	Principal Intermediates	Reference
TiO_2 Nanotubes	50 mg/50 mL	40 ppm	4	Sun light	100.00%	No report	[61]
$SrFeO_{3-\delta}$	1000 ppm	50 ppm	6	125 W, Mercury Vapor Lamp	99.00%	No report	[62]
TiO **	0.3% *w/v*	300 ppm	4	Sun light	98.50%	3-nitrophenol and 4-nitrophenol	[63]
TiO_2	50 mg	50 ppm	8	125 W, Mercury Vapor Lamp	98.00%	No report	[10]
G-ZnO-Au NCs	4 ppm	5 mM	2.3	500 W, <420 nm	97.80%	Aniline	[64]
(0.50%) Zn doped TiO_2		15 ppm	2	254 nm	97.00%	No report	[65]
GT-1	200 ppm	50 ppm	4	200 W Mercury Vapor Lamp	96.00%	No report	[66]
Ag-h-TiO_2 ***	0.5 g/L	61.5 ppm	3.5	435.8 nm	95.50%	*n*-butanol, di-ethyl ether, furan, orthoformic acid, propanol and acetic acid.	[67]
$TiFe_{0.5}$ ***	4 glass plates	2.51×10^{-4} M	4	320–500 nm	88.45%	No report	[22]
ZnO_2 *	30 ppm	15 ppm	2	254 nm	97.55%	2-NPhs, 3-NPhs and 4-NPhs	This work

Note: G–ZnO–Au NCs = Graphene–ZnO–Au Nanocomposites, GT-1 = Graphitic Carbon (1%)-TiO_2 Composites, Ag–h–TiO_2 = Ag Doped Hollow TiO_2 Nanospheres, TiFe0.5 = 0.5 wt.% Fe-doped TiO_2 deposited as thin film on glass plates (19.5 cm2 irradiation area), Nitrophenol = NPhs, 2-nitrophenol = 2-NPhs, 3-nitrophenol = 3-NPhs and 4-nitrophenol = 4-NPhs.2.4 Degradation Products Identification by High-Resolution Mass Spectrometry. * Acid ** Alkaline *** Neutral (the reactions where the pH is not specified, are assumed to be aqueous solution).

To explore the mechanism of NB photodegradation by ZnO_2 nanoparticles, the possible intermediates formed during the reaction were identified by GC-MS, where 2-nitrophenol (2-NPhs), 3-nitrophenol(3-NPhs) and 4-nitrophenol(4-NPhs) were detected to be the major products from our nitrobenzene degradation. The NB peak appeared in the GC chromatogram for pH 2 (Figure 8A), 7 (Figure 8B) and 10 (Figure 8C) at a retention time near 5.9 min, whereas the peaks corresponding to the intermediates appeared at retention times near 6.2 min (same retention time for all three pHs). Figure 9 shows the mass spectrum result of the mentioned peaks, which were assigned to NB (A), 2-NPhs (B), 3-NPhs (C) and 4-NPhs (D), respectively. The concentration of the intermediates was measured by calculating the area under the curve from the chromatogram peaks in proportion to the known NB concentration. The reaction intermediates detected for the pH 2 (Figure 8A), 7 (Figure 8B) and 10 (Figure 8C) were 0.51%, 6.3% and 1.2% respectively.

Rendering these products, it is proposed that nitrobenzene could be oxidized through one pathway, and hydroxyl radicals could be added onto the aromatic ring of nitrobenzene and form hydroxy cyclohexadienyl radicals [68,69].

The hydroxy cyclohexadienyl radicals by oxidation or disproportionation could produce 2-nitrophenol, 3-nitrophenol, and 4-nitrophenol, depending on the position (*ortho*, *meta*, *para*) of the aromatic ring of NB it was added on to. However, the nitrophenol distribution does not correlate with the deactivating characteristics of the nitro group [70].

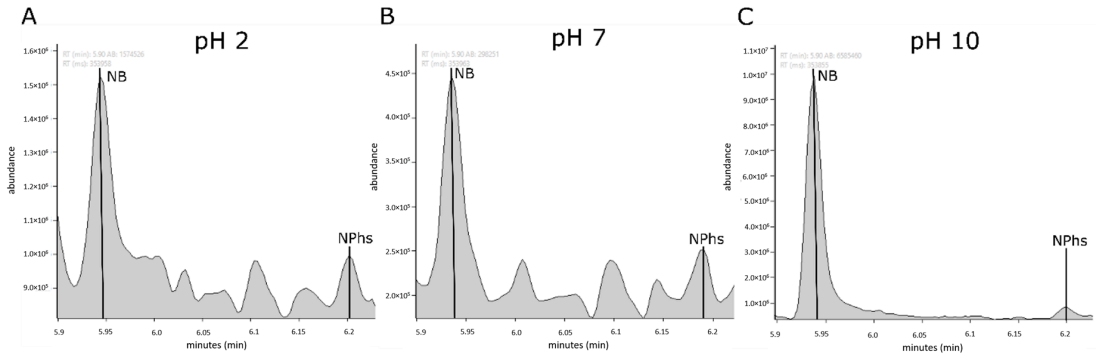

Figure 8. Gas chromatography (GC) chromatograms of the NB photocatalysis extracts for the reactions at pH: (**A**) 2, (**B**) 7 and (**C**) 10. The two peaks were detected to be NB and reaction intermediaries, nitrophenols (NPhs).

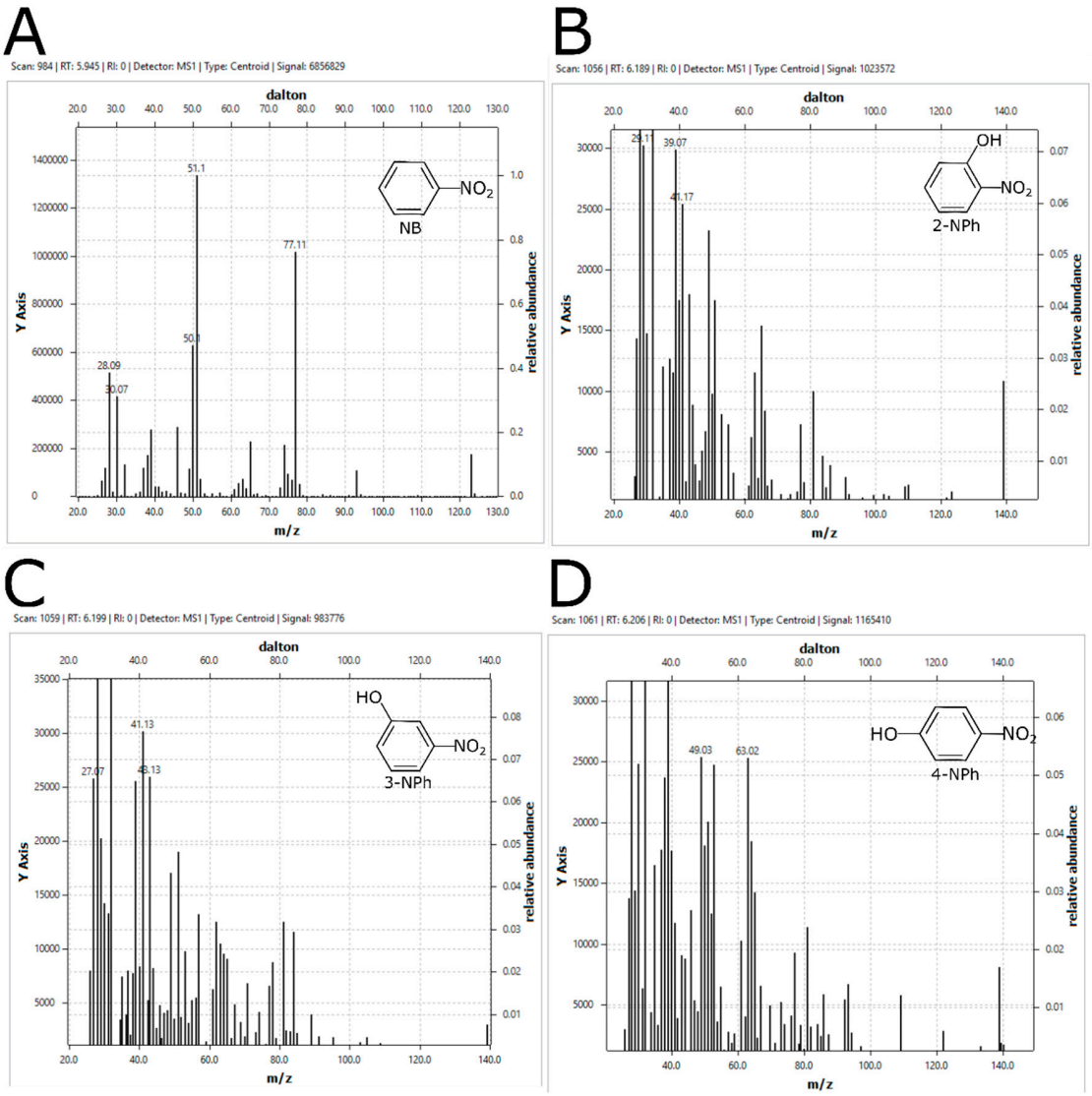

Figure 9. Mass spectrum (MS) for the detected molecules of the NB photocatalysis extracts. (**A**) NB, (**B**) 2-nitrophenol (2-NPh), (**C**) 3-nitrophenol (3-NPh) and (**D**) 4-nitrophenol (4-NPh) (NPs).

This result confirms the role of the hydroxyl radical as an initiator of the oxidative reaction, supporting a mineralization and the mechanism stated at Equations (6)–(11). However,

further experiments should be made to completely elucidate the mineralization mechanism of NB's photodegradation by ZnO_2 nanoparticles.

3. Materials and Methods

3.1. Synthesis of ZnO_2 Nanoparticles

The ZnO_2 nanoparticles were synthesized by a sol-gel/sonochemical route; for this purpose, a precursor solution of 50 mL was prepared using 5 mL of 30% peroxide with HPLC grade water from J.T Baker, the solution was sonicated (TPC Advance Technology UC-450 Model) in 2 min. Then, 1 g of zinc acetate (99.9%) from TSA reagents was dissolved in the precursor solution by ultrasonication for 5 min until a homogeneous solution is obtained. Subsequently it was sonicated for half an hour at a temperature of 60 ± 5 °C. Once this time elapsed a white suspension was obtained [31]. This solution was placed in a Petri dish and allowed to dry at 36 °C for 24 h. A white powder was obtained which was washed twice with excess distilled water for the synthesis of ZnO_2 nanoparticles.

3.2. Characterization of ZnO_2 Nanoparticles

3.2.1. UV-VIS Spectroscopy

To evaluate the optical properties of the nanoparticles and try to understand the electronic structure that the nanoparticles could have, a HACH UV-VIS DR 6000 spectrophotometer (Dusseldorf, Germany) was used and a 30 ppm solution of ZnO_2 nanoparticles dissolved in water was read. The obtained spectrum was made in a sweeping range and 1 cm quartz cells were used.

3.2.2. FT-IR Analysis

To study the binding vibrations of ZnO_2, FT-IR analysis was employed. The spectrum was obtained by Nicolet IS10 Thermo Scientific FT-IR equipment (Waltham, MA, USA), with the ATR method in a sweep of 500 cm^{-1} to 4000 cm^{-1} (100 scans were performed per reading and 3 readings were carried out). Usually approximately 100 mg of powder sample was used.

3.2.3. Raman Analysis

The Raman spectrum was recorded using a Raman WITec Confocal Raman Microscope System (alpha300R, Witec Inc., Ulm, German) using an Nd: YVO4 laser with an excitation wavelength of 532 nm. The typical resolution used was achieved using a 100x objective with a grid of 672 lines/mm (4 cm^{-1}) and a grid of 1800 lines/mm (1 cm^{-1}). The rate of acquisition of point spectra was ≤10 µs, using a lamp power of 14.4 mW (118 µm). Considering the effects of laser temperature on the sample the spectra were corrected using a linear function.

3.2.4. X-ray Diffraction (XRD)

X-ray powder diffraction experiments were performed on a Brucker D8 Advance diffractometer (Bruker Co., Billerica, MA, USA) in the range of 15–75° (2θ) in step sizes of 0.02, with a scanning speed of 0.02°/1.2004 s. The radiation tube of Cu Kα (1.5406 Å) was operated at 30 kV and 30 mA.

3.2.5. Scanning Electronic Microscope (SEM)

The sample was analyzed with a gold coating to improve the resolution of the image. For the coating the sputtering method was followed (JFC−110 ion sputter, JEOL). The samples images were obtained in a scanning electron microscope (JEOL JSM7600F Tokyo, Japan) with an accelerating voltage of 5 keV. The size distribution and average grain and crystal diameter size were determined by counting the grains and crystals with an image processing and analysis software ImageJ for counting and the software for graphics and data analysis origin pro 8 for size distribution. The average diameter of each particle and crystal was determined by the measurement of at least 180–200 particles or crystals per

image from 5 images. Besides, an energy dispersion spectroscopy analysis (EDS) was carried out for the chemical composition of the material using the same electron microscope (JEOL JSM7600F) with a range of operating voltage from 0–12 keV.

3.2.6. DLS Analysis and Zeta Potential

The dynamic light scattering (DLS) measurements to obtain the hydrodynamic diameter (D_h) were carried out at room temperature (25 °C) using a Zetasizer nano-ZS from Malvern Instruments (ZEN3500, Worcestershire, UK). The same equipment was used to measure the zeta potential (ζ) at different pH values adjusted with HCl and NaOH. Both the D_h and ζ measurements were evaluated at room temperature using a 300 ppm ZnO_2 nanoparticle suspension.

3.3. Photocatalytic Degradation of Nitrobenzene

The reaction conditions to measure the photocatalytic activity of the ZnO_2 nanoparticles for NB degradation are specified by Reynoso-Soto et al. (2013) [65]. Briefly, for the photocatalysis reactions the solution prepared was 250 mL of NB at 15 ppm and ZnO_2 nanoparticles at 20, 30 and 40 ppm at a neutral pH unless specified. The samples were centrifuged in a microcentrifuge (Thermo Espresso Personal Microcentrifuge, Thermo Fisher Scientific Inc., MA, USA) for 10 min at 15 rpm to remove the nanoparticles from the solution. For the pH modifications, HCl and NaOH were used. All the photocatalysis experiments were done in duplicate. The specific energy consumption (SEC) was estimated and the following expression (Equation (11)) was used:

$$SEC = L \times NP \times t/m \quad (11)$$

where L = number of lamps, NP = nominal power of lamps (KW), t = time for maximum percentage of degradation (h) and m = mass of NB degraded (kg), which was calculated from the initial concentration of NB and the concentration of NB at "t" [71].

To identify the degradation intermediates of the NB photocatalysis degradation, gas chromatography–mass spectrometry (GC-MS) was applied. GC-MS were recorded on a Thermo Scientific TRACE 1310 (GC) and Thermo Scientific single quadrupole ISQ LT (MS), with a column model TG-SQC (30 m × 0.25 mm inner diameter, 0.25 μm film thickness). The detector temperature was 240 °C, the injector temperature was 250 °C, and transfer line temperature was 250 °C; oven temperature started at 70 °C for 3 min, increased at a 40 °C/min rate until 280 °C, with a hold time of 7 min. Helium was employed as a carrier gas, at 1 mL/min flow. Samples of 50 mL were extracted with 5 mL dichloromethane (duplicate), at a 10:1 ratio between sample and solvent. The organic extract was dried with anhydrous Na_2SO_4. One milliliter of the extract was placed in a 2 mL vial and then it was manually injected to GC.

The percentage of the degradation products detected was calculated using the area under the curve of the chromatogram peaks corresponding to NB and the nitrophenols (NPhs) in proportion to the NB% detected by UV-Vis spectroscopy. The percentage of reaction intermediates corresponds to the sum of these.

4. Conclusions

In this study we synthesized ZnO_2 nanoparticles by a sol-gel/sonochemical route and its photocatalytic activity was evaluated by NB degradation. The synthesized nanoparticles have a crystal size of ~6 nm which cluster to form particles of 100 nm, with good dispersion in water having a positive ζ (+15 mV) at pH = 6.3 and an IEP (pH = 3–3.5) and PZC (pH = 7.5–8). ZnO_2 nanoparticles presented great results as a photocatalyst, being more effective at a pH = 2 and a concentration ratio of 2:1 (nanoparticle: NB), with a SEC of approx. 60,000 kWh/kg. The combination of the electron–hole formed in the nanoparticle and an unpaired electron is highly active, which is this the key to start a hydroxylation reaction. This guides us to propose a further investigation of these aspects that will help

us have a better understanding of the mechanism of reaction due to the intermediates detected by GC-MS. The GC-MS analysis shows that 2-nitrophenol, 3-nitrophenol, and 4-nitrophenol were the principal hydroxylated intermediates detected. The observed catalyst potential of ZnO_2 nanoparticles opens exciting possibilities for exploring this synthesis route and optimizes the activity of this catalyst.

Author Contributions: Conceptualization, J.I.D.L.R. and V.A.R.V.; methodology, S.P.S.; software, V.A.R.V.; validation, J.I.D.L.R., V.A.R.V. and E.H.G.; formal analysis, J.I.D.L.R.; investigation, J.I.D.L.R.; resources, J.I.D.L.R.; data curation, V.A.R.V.; writing—original draft preparation, J.I.D.L.R.; writing—review and editing, V.A.R.V., J.I.D.L.R., S.P.S.; visualization, S.P.S.; supervision, S.P.S., B.L.S.; project administration, B.L.S.; funding acquisition B.L.S., M.D.C.B.P. All authors have read and agreed to the published version of the manuscript.

Funding: This work was supported by the National Council of Science and Technology (CONACYT) [CB2015-253128].

Acknowledgments: We would like to acknowledge Adriana Tejeda (IIM-UNAM) for the support in carrying out X-ray measurements; Omar Novelo (IIM-UNAM) for the support in the scanning electron microscopy characterization, María Elena Villafuerte Castrejón (IIM-UNAM) and Gerardo Cesar Diaz Trujillo (UABC) for an investigation residency in the Investigation Institute of Materials (IIM) and Arturo Estolano (UABC) for the support in the gas chromatography–mass spectrum analysis.

Conflicts of Interest: The authors declare no conflict of interest.

References

1. Beauchamp, R.O.; Irons, R.D.; Rickert, D.E.; Couch, D.B.; Hamm, T.E.; Lyon, J.P. A critical review of the literature on nitrobenzene toxicity. *Crit. Rev. Toxicol.* **1982**, *11*, 33–84. [CrossRef]
2. Katritzky, A.R.; Oliferenko, P.; Oliferenko, A.; Lomaka, A.; Karelson, M. Nitrobenzene toxicity: QSAR correlations and mechanistic interpretations. *J. Phys. Org. Chem.* **2003**, *16*, 811–817. [CrossRef]
3. Harrison, M.R. Toxic methaemoglobinaemia. *Anaesthesia* **1977**, *32*, 270–272. [CrossRef] [PubMed]
4. Mu, Y.; Yu, H.Q.; Zheng, J.C.; Zhang, S.J.; Sheng, G.P. Reductive degradation of nitrobenzene in aqueous solution by zero-valent iron. *Chemosphere* **2004**, *54*, 789–794. [CrossRef] [PubMed]
5. Wang, C.; Feng, Y.; Zhao, S.; Li, B.L. A dynamic contaminant fate model of organic compound: A case study of Nitrobenzene pollution in Songhua River, China. *Chemosphere* **2012**, *88*, 69–76. [CrossRef] [PubMed]
6. Cai, Z.; Fu, J.; Du, P.; Zhao, X.; Hao, X.; Liu, W.; Zhao, D. Reduction of nitrobenzene in aqueous and soil phases using carboxymethyl cellulose stabilized zero-valent iron nanoparticles. *Chem. Eng. J.* **2018**, *332*, 227–236. [CrossRef]
7. Elnashaie, S.S.E.; Danafar, F.; Abashar, M.E.E. Maximum Production Minimum Pollution (MPMP), Necessary but not Sufficient for Sustainability. *Eur. J. Sustain. Dev. Res.* **2018**, *2*, 41. [CrossRef]
8. Zhao, L.; Lu, Z.; Tan, S.; Ciren, J.; Tan, C. Effects of glucose and starch on the toxicity of nitrobenzene to plants and microbes in constructed wetlands. *Sci. Total Environ.* **2019**, *658*, 809–817. [CrossRef]
9. Liu, L.-L.; Chen, J.; Yu, C.-X.; Lv, W.-X.; Yu, H.-Y.; Cui, X.-Q.; Liu, L. A novel Ag (I)-calix[4]arene coordination polymer for the sensitive detection and efficient photodegradation of nitrobenzene in aqueous solution. *Dalt. Trans.* **2017**, *46*, 178–185. [CrossRef]
10. Tayade, R.J.; Kulkarni, R.G.; Jasra, R.V. Photocatalytic degradation of aqueous nitrobenzene by nanocrystalline TiO_2. *Ind. Eng. Chem. Res.* **2006**, *45*, 922–927. [CrossRef]
11. Cao, L.; Zhang, C.; Zou, S.; Zhu, G.; Li, N.; Zhang, Y.; Rittmann, B.E. Simultaneous anaerobic and aerobic transformations of nitrobenzene. *J. Environ. Manag.* **2018**, *226*, 264–269. [CrossRef] [PubMed]
12. Li, Y.P.; Cao, H.B.; Liu, C.M.; Zhang, Y. Electrochemical reduction of nitrobenzene at carbon nanotube electrode. *J. Hazard. Mater.* **2007**, *148*, 158–163. [CrossRef] [PubMed]
13. Chong, H.; Li, P.; Xiang, J.; Fu, F.; Zhang, D.; Ran, X.; Zhu, M. Design of an ultrasmall Au nanocluster-CeO_2 mesoporous nanocomposite catalyst for nitrobenzene reduction. *Nanoscale* **2013**, *5*, 7622–7628. [CrossRef] [PubMed]
14. Caprio, V.; Insola, A.; Volpiceli, G. Ozonation of Aqueous Solutions of Nitrobenzene. *Ozone Sci. Eng.* **2008**, *6*, 115–121. [CrossRef]
15. Nishino, S.F.; Spain, J.C. Oxidative pathway for the biodegradation of nitrobenzene by *Comamonas* sp. strain JS765. *Appl. Environ. Microbiol.* **1995**, *61*, 2308–2313. [CrossRef]
16. Wang, D.; Shan, H.; Sun, X.; Zhang, H.; Wu, Y. Removal of nitrobenzene from aqueous solution by adsorption onto carbonized sugarcane bagasse. *Adsorpt. Sci. Technol.* **2018**, *36*, 1366–1385. [CrossRef]

17. Priya, M.H.; Madras, G. Photocatalytic degradation of nitrobenzenes with combustion synthesized nano-TiO_2. *J. Photochem. Photobiol. A Chem.* **2006**, *178*, 1–7. [CrossRef]
18. Bhatkhande, D.S.; Pangarkar, V.G.; Beenackers, A.A.C.M. Photocatalytic degradation for environmental applications—A review. *J. Chem. Technol. Biotechnol.* **2002**, *77*, 102–116. [CrossRef]
19. Wolanov, Y.; Prikhodchenko, P.V.; Medvedev, A.G.; Pedahzur, R.; Lev, O. Zinc Dioxide Nanoparticulates: A Hydrogen Peroxide Source at Moderate pH. *Environ. Sci. Technol.* **2013**, *47*, 8769–8774. [CrossRef]
20. Rodríguez, M.; Kirchner, A.; Contreras, S.; Chamarro, E.; Esplugas, S. Influence of H_2O_2 and Fe(III) in the photodegradation of nitrobenzene. *J. Photochem. Photobiol. A Chem.* **2000**, *133*, 123–127. [CrossRef]
21. Contreras, S.; Rodríguez, M.; Chamarro, E.; Esplugas, S.; Casado, J. Oxidation of nitrobenzene by O3/UV: The influence of H_2O_2 and Fe(III). Experiences in a pilot plant. *Water Sci. Technol.* **2001**, *44*, 39–46. [CrossRef] [PubMed]
22. Lee, K.M.; Lai, C.W.; Ngai, K.S.; Juan, J.C. Recent developments of zinc oxide based photocatalyst in water treatment technology: A review. *Water Res.* **2016**, *88*, 428–448. [CrossRef] [PubMed]
23. Rej, S.; Mascaretti, L.; Santiago, E.Y.; Tomanec, O.; Kment, Š.; Wang, Z.; Zbořil, R.; Fornasiero, P.; Govorov, A.O.; Naldoni, A. Determining Plasmonic Hot Electrons and Photothermal Effects during H2 Evolution with TiN-Pt Nanohybrids. *ACS Catal.* **2020**, *10*, 5261–5271. [CrossRef]
24. Crişan, M.; Mardare, D.; Ianculescu, A.; Drăgan, N.; Niţoi, I.; Crişan, D.; Voicescu, M.; Todan, L.; Oancea, P.; Adomniţei, C.; et al. Iron doped TiO_2 films and their photoactivity in nitrobenzene removal from water. *Appl. Surf. Sci.* **2018**, *455*, 201–215. [CrossRef]
25. Cropek, D.; Kemme, P.A.; Makarova, O.V.; Chen, L.X.; Rajh, T. Selective photocatalytic decomposition of nitrobenzene using surface modified TiO_2 nanoparticles. *J. Phys. Chem. C* **2008**, *112*, 8311–8318. [CrossRef]
26. Ayati, A.; Tanhaei, B.; Bamoharram, F.F.; Ahmadpour, A.; Maydannik, P.; Sillanpää, M. Photocatalytic degradation of nitrobenzene by gold nanoparticles decorated polyoxometalate immobilized TiO_2 nanotubes. *Sep. Purif. Technol.* **2016**, *171*, 62–68. [CrossRef]
27. Chen, W.; Lu, Y.H.; Wang, M.; Kroner, L.; Paul, H.; Fecht, H.-J.; Bednarcik, J.; Stahl, K.; Zhang, Z.L.; Wiedwald, U.; et al. Synthesis, Thermal Stability and Properties of ZnO_2 Nanoparticles. *J. Phys. Chem. C.* **2009**, *113*, 1320–1324. [CrossRef]
28. Verma, S.; Jain, S.L. Nanosized zinc peroxide (ZnO_2): A novel inorganic oxidant for the oxidation of aromatic alcohols to carbonyl compounds. *Inorg. Chem. Front.* **2014**, *1*, 534. [CrossRef]
29. Hsu, C.C.; Wu, N.L. Synthesis and photocatalytic activity of ZnO/ZnO2 composite. *J. Photochem. Photobiol. A Chem.* **2005**, *172*, 269–274. [CrossRef]
30. Giannakoudakis, D.A.; Florent, M.; Wallace, R.; Secor, J.; Karwacki, C.; Bandosz, T.J. Zinc peroxide nanoparticles: Surface, chemical and optical properties and the effect of thermal treatment on the detoxification of mustard gas. *Appl. Catal. B Environ.* **2018**, *226*, 429–440. [CrossRef]
31. Profesional, E.; Física, D.E.I.; Carlos, R.; Surichaqui, C. Sintesis y Caracterización de nanopartículas de Zn02 y su actividad antímicrobiana. *EsESCUELA Prof. Ing. FÍSICA* **2013**, *84*. [CrossRef]
32. Gondal, M.A.; Drmosh, Q.A.; Yamani, Z.H.; Saleh, T.A. Synthesis of ZnO_2 nanoparticles by laser ablation in liquid and their annealing transformation into ZnO nanoparticles. *Appl. Surf. Sci.* **2009**, *256*, 298–304. [CrossRef]
33. Drmosh, Q.A.; Gondal, M.A.; Yamani, Z.H.; Saleh, T.A. Spectroscopic characterization approach to study surfactants effect on ZnO_2 nanoparticles synthesis by laser ablation process. *Appl. Surf. Sci.* **2010**, *256*, 4661–4666. [CrossRef]
34. Mallika, A.N.; Ramachandrareddy, A.; Sowribabu, K.; Reddy, K.V. Synthesis and optical characterization of aluminum doped ZnO nanoparticles. *Ceram. Int.* **2014**, *40*, 12171–12177. [CrossRef]
35. Rusdi, R.; Rahman, A.A.; Mohamed, N.S.; Kamarudin, N.; Kamarulzaman, N. Preparation and band gap energies of ZnO nanotubes, nanorods and spherical nanostructures. *Powder Technol.* **2011**, *210*, 18–22. [CrossRef]
36. Drmosh, Q. Synthesis and Characterization of Nano-Structure Metal Oxides and Peroxides Prepared by Laser Ablation in Liquids. Ph.D. Thesis, King Fahd University of Petroleum and Minerals, Dhahran, Saudi Arabia, 2010.
37. Malhotra, V.M.; Jasty, S.; Mu, R. FT-IR spectra of water in microporous KBr pellets and water's desorption kinetics. *Appl. Spectrosc.* **1989**, *43*, 638–645. [CrossRef]

38. Escobedo-Morales, A.; Esparza, R.; García-Ruiz, A.; Aguilar, A.; Rubio-Rosas, E.; Pérez, R. Structural and vibrational properties of hydrothermally grown ZnO_2 nanoparticles. *J. Cryst. Growth* **2011**, *316*, 37–41. [CrossRef]
39. Yang, L.Y.; Feng, G.P.; Wang, T.X. Green synthesis of ZnO_2 nanoparticles from hydrozincite and hydrogen peroxide at room temperature. *Mater. Lett.* **2010**, *64*, 1647–1649. [CrossRef]
40. de Mello, L.B.; Varanda, L.C.; Sigoli, F.A.; Mazali, I.O. Co-precipitation synthesis of (Zn-Mn)-co-doped magnetite nanoparticles and their application in magnetic hyperthermia. *J. Alloys Compd.* **2019**, 698–705. [CrossRef]
41. Gonçalves, N.S.; Carvalho, J.A.; Lima, Z.M.; Sasaki, J.M. Size-strain study of NiO nanoparticles by X-ray powder diffraction line broadening. *Mater. Lett.* **2012**, *72*, 36–38. [CrossRef]
42. Zak, A.K.; Majid, W.H.A.; Abrishami, M.E.; Yousefi, R. X-ray analysis of ZnO nanoparticles by Williamson-Hall and size-strain plot methods. *Solid State Sci.* **2011**, *13*, 251–256. [CrossRef]
43. Bai, H.; Liu, X. Green hydrothermal synthesis and photoluminescence property of ZnO_2 nanoparticles. *Mater. Lett.* **2010**, *64*, 341–343. [CrossRef]
44. Fatehah, M.O.; Aziz, H.A.; Stoll, S. Stability of ZnO Nanoparticles in Solution. Influence of pH, Dissolution, Aggregation and Disaggregation Effects. *J. Colloid Sci. Biotechnol.* **2014**, *3*, 75–84. [CrossRef]
45. Omar, F.M.; Aziz, H.A.; Stoll, S. Aggregation and disaggregation of ZnO nanoparticles: Influence of pH and adsorption of Suwannee River humic acid. *Sci. Total Environ.* **2013**, *468*, 195–201. [CrossRef]
46. Berg, J.M.; Romoser, A.; Banerjee, N.; Zebda, R.; Sayes, C.M. The relationship between pH and zeta potential of ~30 nm metal oxide nanoparticle suspensions relevant to in vitro toxicological evaluations. *Nanotoxicology* **2009**, *3*, 276–283. [CrossRef]
47. Zhang, Q.; Xu, M.; You, B.; Zhang, Q.; Yuan, H.; Ostrikov, K. Oxygen Vacancy-Mediated ZnO Nanoparticle Photocatalyst for Degradation of Methylene Blue. *Appl. Sci.* **2018**, *8*, 353. [CrossRef]
48. Moon, D.R.; Ingham, T.; Whalley, L.K.; Seakins, P.W.; Baeza-Romero, M.T.; Heard, D.E. Production of HO_2 and OH radicals from near-UV irradiated airborne TiO_2 nanoparticles. *Phys. Chem. Chem. Phys.* **2019**, *21*, 2325–2336. [CrossRef] [PubMed]
49. Zent, A.P.; Ichimura, A.S.; Quinn, R.C.; Harding, H.K. The formation and stability of the superoxide radical (O2-) on rock-forming minerals: Band gaps, hydroxylation state, and implications for mars oxidant chemistry. *J. Geophys. Res.* **2008**, *113*, 1–13. [CrossRef]
50. Wu, W.; Lin, R.; Shen, L.; Liang, R.; Yuan, R.; Wu, L. Highly efficient visible-light-induced photocatalytic hydrogenation of nitrobenzene to aniline in water. *RSC Adv.* **2013**, *3*, 10894–10899. [CrossRef]
51. Modi, K.B.; Natarajan, K.; Kathad, C.R.; Shah, S.J.; Raval, P.Y.; Pathak, T.K.; Meshiya, U.M.; Vyas, K.G.; Bajaj, H.C.; Tayade, R.J. Synthesis and characterization of ferrite-semiconductor nano composite for photocatalytic degradation of aqueous nitrobenzene solution. *AIP Conf. Proc.* **2016**, *1728*, 1–6. [CrossRef]
52. Shahrezaei, F.; Mansouri, Y.; Zinatizadeh, A.A.L.; Akhbari, A. Photocatalytic degradation of aniline using TiO_2 nanoparticles in a vertical circulating photocatalytic reactor. *Int. J. Photoenergy* **2012**, *2012*, 430638. [CrossRef]
53. Flores, S.O.; Rios-Bernij, O.; Valenzuela, M.A. Photocatalytic reduction of nitrobenzene by titanium dioxide powder. *Top. Catal.* **2007**, *44*, 507–511. [CrossRef]
54. Chong, M.N.; Jin, B.; Chow, C.W.K.; Saint, C. Recent developments in photocatalytic water treatment technology: A review. *Water Res.* **2010**, *44*, 2997–3027. [CrossRef]
55. Jeong, S.; Lee, H.; Park, H.; Jeon, K.J.; Park, Y.K.; Jung, S.C. Rapid photocatalytic degradation of nitrobenzene under the simultaneous illumination of UV and microwave radiation fields with a TiO_2 ball catalyst. *Catal. Today* **2018**, *307*, 65–72. [CrossRef]
56. ElMetwally, A.E.; Eshaq, G.; Al-Sabagh, A.M.; Yehia, F.Z.; Philip, C.A.; Moussa, N.A.; ElShafei, G.M.S. Insight into heterogeneous Fenton-sonophotocatalytic degradation of nitrobenzene using metal oxychlorides. *Sep. Purif. Technol.* **2019**, *210*, 452–462. [CrossRef]
57. Bergs, C.; Simon, P.; Prots, Y.; Pich, A. Ultrasmall functional ZnO_2 nanoparticles: Synthesis, characterization and oxygen release properties. *RSC Adv.* **2016**, *6*, 84777–84786. [CrossRef]
58. Bergs, C.; Brück, L.; Rosencrantz, R.R.; Conrads, G.; Elling, L.; Pich, A. Biofunctionalized zinc peroxide (ZnO_2) nanoparticles as active oxygen sources and antibacterial agents. *RSC Adv.* **2017**, *7*, 38998–39010. [CrossRef]

59. Karthik, R.; Govindasamy, M.; Chen, S.M.; Cheng, Y.H.; Muthukrishnan, P.; Padmavathy, S.; Elangovan, A. Biosynthesis of silver nanoparticles by using Camellia japonica leaf extract for the electrocatalytic reduction of nitrobenzene and photocatalytic degradation of Eosin-Y. *J. Photochem. Photobiol. B Biol.* **2017**, *170*, 164–172. [CrossRef]
60. Lawrence, A.; Thollander, P.; Andrei, M.; Karlsson, M. Specific Energy Consumption/Use (SEC) in Energy Management for Improving Energy Efficiency in Industry: Meaning, Usage and Differences. *Energies* **2019**, *12*, 247. [CrossRef]
61. Tayade, R.J.; Key, D.L. Synthesis and Characterization of Titanium Dioxide Nanotubes for Photocatalytic Degradation of Aqueous Nitrobenzene in the Presence of Sunlight. *Mater. Sci. Forum.* **2010**, *657*, 62–74. [CrossRef]
62. Srilakshmi, C.; Saraf, R.; Shivakumara, C. Effective degradation of aqueous nitrobenzene using the SrFeO3−δ photocatalyst under UV illumination and its kinetics and mechanistic studies. *Ind. Eng. Chem. Res.* **2015**, *54*, 7800–7810. [CrossRef]
63. Bhatkhande, D.S.; Pangarkar, V.G.; Beenackers, A.A.C.M. Photocatalytic degradation of nitrobenzene using titanium dioxide and concentrated solar radiation: Chemical effects and scaleup. *Water Res.* **2003**, *37*, 1223–1230. [CrossRef]
64. Roy, P.; Periasamy, A.P.; Liang, C.T.; Chang, H.T. Synthesis of graphene-ZnO-Au nanocomposites for efficient photocatalytic reduction of nitrobenzene. *Environ. Sci. Technol.* **2013**, *47*, 6688–6695. [CrossRef] [PubMed]
65. Reynoso-Soto, E.A.; Pérez-Sicairos, S.; Reyes-Cruzaley, A.P.; Castro-Riquelme, C.L.; Félix-Navarro, R.M.; Paraguay-Delgado, F.; Alonso-Núñez, G.; Lin-Ho, S.W. Photocatalytic degradation of nitrobenzene using nanocrystalline TiO2 photocatalyst doped with Zn ions. *J. Mex. Chem. Soc.* **2013**, *57*, 298–305. [CrossRef]
66. Jo, W.K.; Won, Y.; Hwang, I.; Tayade, R.J. Enhanced photocatalytic degradation of aqueous nitrobenzene using graphitic carbon-TiO2 composites. *Ind. Eng. Chem. Res.* **2014**, *53*, 3455–3461. [CrossRef]
67. Boxi, S.S.; Paria, S. Visible light induced enhanced photocatalytic degradation of organic pollutants in aqueous media using Ag doped hollow TiO2 nanospheres. *RSC Adv.* **2015**, *5*, 37647–37668. [CrossRef]
68. Bhatia, K. Hydroxyl radical induced oxidation of nitrobenzene. *J. Phys. Chem.* **1975**, *79*, 1032–1038. [CrossRef]
69. Eberhardt, M.K.; Yoshida, M. Radiation-induced homolytic aromatic substitution. I. Hydroxylation of nitrobenzene, chlorobenzene, and toluene. *J. Phys. Chem.* **1973**, *77*, 589–597. [CrossRef]
70. Zhang, Y.; Zhang, K.; Dai, C.; Zhou, X.; Si, H. An enhanced Fenton reaction catalyzed by natural heterogeneous pyrite for nitrobenzene degradation in an aqueous solution. *Chem. Eng. J.* **2014**, *244*, 438–445. [CrossRef]
71. Pérez-Sicairos, S.; Corrales-López, K.A.; Hernández-Calderón, O.M.; Salazar-Gastélum, M.I.; Félix-Navarro, R.M. Photochemical Degradation of Nitrobenzene by S2O8–2 Ions and UV Radiation. *Rev. Int. Contam. Ambient.* **2016**, *32*, 227–236. [CrossRef]

© 2020 by the authors. Licensee MDPI, Basel, Switzerland. This article is an open access article distributed under the terms and conditions of the Creative Commons Attribution (CC BY) license (http://creativecommons.org/licenses/by/4.0/).